ACS APPLIED MATERIALS & INTERFACES

Research Article

www.acsami.org

Palladium/Single-Walled Carbon Nanotube Back-to-Back Schottky Contact-Based Hydrogen Sensors and Their Sensing Mechanism

Miluo Zhang,[†] Lauren L. Brooks,[†] Nicha Chartuprayoon,[†] Wayne Bosze,[†] Yong-ho Choa,[‡] and Nosang V. Myung*[,†]

[†]Department of Chemical and Environmental Engineering and Center for Nanoscale Science and Engineering, University of California—Riverside, Riverside, California 92521, United States

[‡]Department of Fine Chemical Engineering/Bionano Technology, Hanyang University, Ansan 426-791, Korea

ABSTRACT: A Schottky contact-based hydrogen (H_2) gas sensor operable at room temperature was constructed by assembling single-walled carbon nanotubes (SWNTs) on a Si/SiO_2 substrate bridged by Pd microelectrodes in a chemiresistive/chemical field effect transistor (chemFET) configuration. The Schottky barrier (SB) is formed by exposing the Pd−SWNT interfacial contacts to H_2 gas, the analyte it was designed to detect. Because a Schottky barrier height (SBH) acts as an exponential bottleneck to current flow, the electrical response of the sensor can be particularly sensitive to small changes in SBH, yielding an enhanced response to H_2 gas. The sensing mechanism was analyzed by $I-V$ and FET properties before and during H_2 exposure. $I-V_{sd}$ characteristics clearly displayed an equivalent back-to-back Schottky diode configuration and demonstrated the formation of a SB during H_2 exposure. The $I-V_g$ characteristics revealed a decrease in the carrier mobility without a change in carrier concentration; thus, it corroborates that modulation of a SB via H_2 adsorption at the Pd−SWNT interface is the main sensing mechanism.

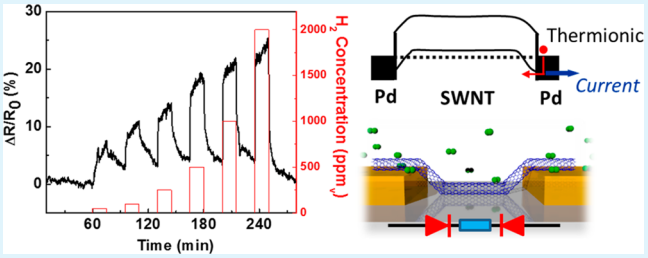

KEYWORDS: *Schottky contact, hydrogen (H_2) gas sensor, Pd, single-walled carbon nanotubes (SWNTs), response time*

1. INTRODUCTION

Hydrogen (H_2) is a potentially emission-free alternative fuel that is considered to be an ideal energy carrier in the foreseeable future. Rapid and accurate H_2 sensors with a low detection limit have been of significant interest and in high demand for safety concerns due to hydrogen's low spark ignition energy (0.017 mJ) and wide flammable range (4−75%).[1] Several types of H_2 sensors[2] have been developed based on metal oxides such as In_2O_3,[3] SnO_2,[4] ZnO,[5] NiO,[6] and TiO_2.[7] However, each selective gas response requires a well-controlled specific high temperature (a few hundred °C) to achieve optimal sensitivity. While elevating the temperature of the sensor accelerates the transport of gases, thus improving both response and recovery times, it can also increase power consumption and device complexity.

Palladium (Pd) has been found to be an excellent sensing material for H_2 due to its catalytic properties and high solubility toward H_2 under ambient conditions. It has been reported that the reversible formation of palladium hydride (PdH_x) is the determining factor for Pd-based sensors, where any number of effects could be exploited, including modulating its lattice constant,[8] conductivity,[9] work function,[10] or optical properties.[11] Pd sensors that take advantage of H_2-induced modulation in resistance show good sensitivity but suffer from delayed response and recovery times due to slow gas transport processes. Pd nanocluster-based H_2 sensors exploiting a H_2-induced lattice expansion show improved sensor response times but albeit at the expense of low sensitivity.[8]

Schottky contact-based H_2 sensors focus on the contact area between the Pd electrode and the semiconductor, where the modulation of contact barrier height is the key factor in determining the performance of a sensor. A metal−semiconductor interface can possess rectifying or nonrectifying energy levels, namely, Schottky or ohmic contacts, respectively. In an ohmic contact, resistance is inversely proportional to the cross sectional area perpendicular to the current and the charge carriers can flow in either direction without rectification under an applied potential. In an ohmic contact-based sensor, the interface resistivity is made as low and as stable as possible to place emphasis on the signal contribution coming from the semiconductor itself. For a rectifying SB contact-based sensor, the opposite effects are required. Because a SBH acts as an exponential limit to current flow in accordance with the law of thermionic emission,[12] the aim of making the modulation of SBH, the key factor in performance, can be achieved by making the SBH a dynamic, sensitive and reversible function of the target analyte concentration. An exponential dependence on a key factor naturally overrides a linear dependency, yielding an enhanced sensitivity sensor. This corroborates the fact that

Received: October 2, 2013
Accepted: December 11, 2013
Published: December 11, 2013

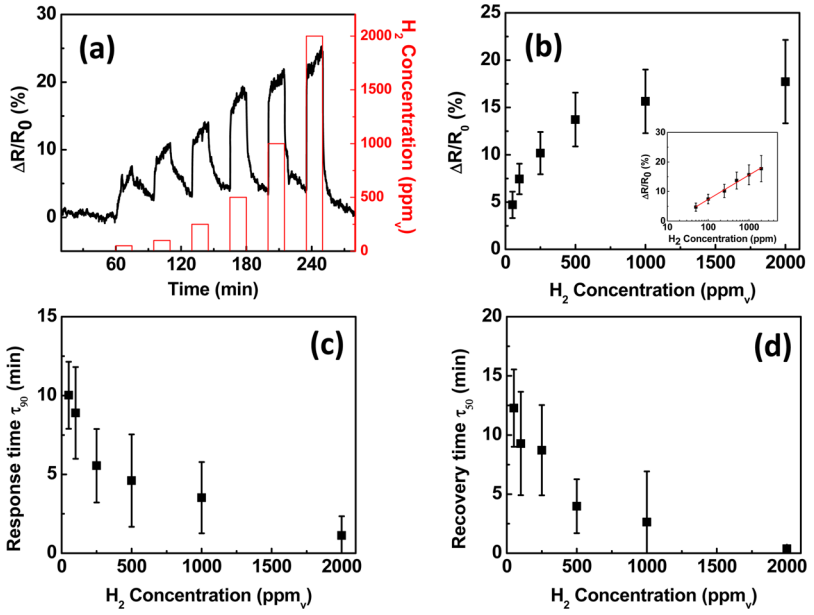

Figure 1. (a) Real-time sensing response, (b) calibration curve, (c) response time, and (d) recovery time of AC aligned SWNTs on Pd microelectrodes toward H_2 at different concentrations. The sensing performance including sensitivity, response time, and recovery time are characterized based on a sample number of 14.

Schottky contact-base sensors have been found to show higher sensitivities to analyte gases than ohmic contact-based sensors. In accordance with the Schottky–Mott model, there is a linear dependence between the SBH and the metal work function. Thus, modulation in the metal work function leads to a direct modulation in the SBH in the metal–semiconductor junction, causing an exponential change in the conductance of the sensor.

Over the past few decades, Schottky contact-based H_2 sensors have been fabricated by the utilization of Pd with various semiconductors, such as Si,[13] TiO_2,[14] and SnO_2.[15] Although a vast improvement in sensitivity and low detection limits have been achieved within these configurations, the SBH on most semiconductors are found to have a much weaker dependence on the metal work function than the Schottky–Mott model suggests. This phenomenon, known as Fermi level pinning, where interface states tend to pin the center of the band gap to the Fermi level, along with undesired compound formation,[13] reduces the expected SBH and thus diminishing the sensor performance.

Carbon nanotubes (CNTs) have been of significant interest owing to their unique electrical, physical, mechanical, and chemical properties, leading to a wide array of applications, including supercapacitors, electrodes, field emission devices, sensors, and other nanoelectronic devices.[16] By taking advantage of its quasi-one-dimensional (1-D) transport properties, CNTs have been widely used as chemiresistive/ChemFETs gas sensors, offering the potential to outperform the established two-dimensional (2-D) thick- and thin-film sensors.[10] In particular, weak Fermi level pinning is anticipated in a metal–CNT contact because the pinning charge has to compete with the large charge density at the van Hove singularities in the density of states of CNTs.[17] In other words, the SBH should be completely controlled by the metal work function in a metal–CNT contact (i.e., display Schottky–Mott model behavior). This is in strong contrast to most bulk metal–semiconductor junctions where Fermi level pinning often dominates the SBH.[17]

In this work, we study the effects of p-type SWNTs in contact with Pd electrodes and show that the development of SBs at the contacts under H_2 exposure enhances their sensing performances. The sensing mechanism was confirmed by I–V and FET properties characterization before and during H_2 exposure. Even though the modulation of the SBH by H_2 has already been reported for a Pd–CNT contact,[10] a H_2 sensor based on this configuration with high sensitivity and fast response/recovery time has not been demonstrated. The Pd–SWNTs sensor showed an enhanced sensing performance when contrasted with other aligned SWNTs made with Pt, Cr, and Au microelectrodes.

2. EXPERIMENTAL SECTION

Detailed information on these sensor configurations have been described in our recently published paper.[18] Briefly, various metal microelectrodes including Pd, Pt, Cr, and Au patterned on oxidized Si substrates (with a SiO_2 thickness of 300 nm) were fabricated via lift-off photolithography processes. Prior to use, prefabricated microelectrode chips were sonicated in nanopure water, followed by an acetone rinse to remove residues. The CNT suspension was prepared by adding 0.2 mg of commercially available carboxylated SWNTs (Carbon Solution, Inc. Riverside, CA) in 20 mL of *N*,*N*-dimethylformamide (DMF, Sigma Aldrich, MO) and sonicating the mixture solution for 90 min until a well-dispersed solution was obtained. The supernatant of the suspended SWNTs solution was collected after centrifuging at 15,000 rpm for 90 min.

To accurately align SWNTs across a prefabricated microelectrode, a customized Teflon cell was employed to hold the microelectrode chip and confine the suspended SWNTs solution for the AC dielectrophoretic alignment. The electrical connection between the external electronic equipment and the microelectrode chip was obtained by clipping the chip with two 32 pin SOIC test clips purchased from Pomona Electronics. Afterwards, 200 μL of the supernatant was placed into the Teflon cell with the chip held for SWNT alignment. To obtain optimized SWNT alignment, a 2 peak to peak voltage (V_{pp}) at 4 MHz frequency was applied to the electrodes for an average of 10 s. A Labview program was designed to command the Keithley 3390 AC generator (aligner) and custom-made DAQ switcher for sequential SWNT alignment. The synthesized sensors were rinsed with nanopure

dx.doi.org/10.1021/am404328g | ACS Appl. Mater. Interfaces 2014, 6, 319–326

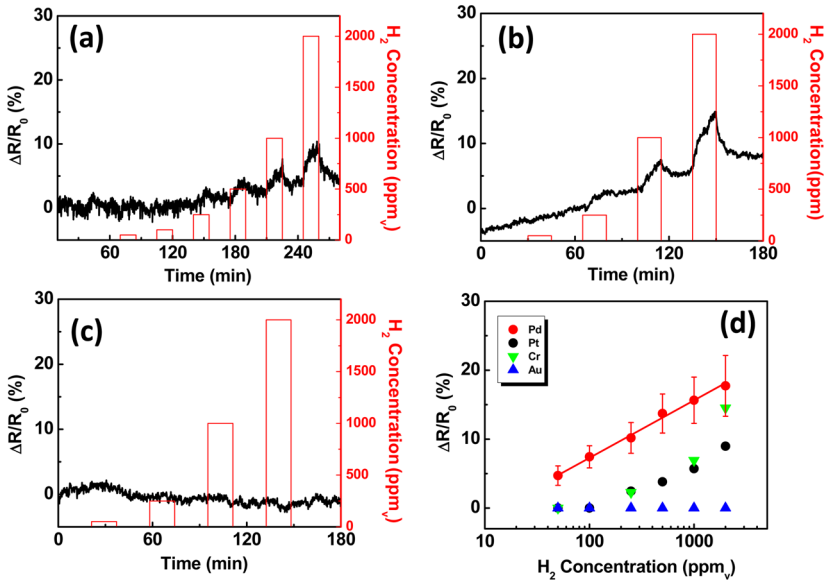

Figure 2. (a–c) Real-time sensing response and (d) calibration curves of AC aligned SWNTs on (a) Pt, (b) Cr, and (c) Au electrodes toward H_2 at different concentration.

water, dried with ultra-pure N_2 gas, and then annealed at 300 °C for 2 h in forming gas.

Back-gated FET properties ($I-V_g$ characteristics) were measured by sweeping the gate voltage from −20 V to +20 V with a fixed source-drain voltage of 1 V during exposures of dry air and 2000 ppm_v H_2 gas in dry air, respectively. Furthermore, the sensing performance was investigated by assembling the sensing chip in a sealed Teflon sensing cell with gas inlet and outlet ports for gas flow and then clipping the chip to a Keithley 236 source measurement to obtain the electrical connection. An applied potential of 1 V was given to each sensor and the resistance was continuously monitored every 0.2 s for the 15 sensors by a custom-made LabView program. H_2 gas was first diluted in dry air to various concentrations and then introduced into the Teflon cell at a total gas flow of 200 sccm for gas sensing measurements.

3. RESULTS AND DISCUSSION

The sensing performance to H_2 adsorption on the aligned SWNTs bridged across the Pd microelectrodes configured as chemiresistors was investigated at room temperature. These sensors were sequentially tested with varied concentrations of H_2 gas ranging from 50 to 2000 ppm_v with a period of H_2 exposure for 15 min and a period with dried air for 20 minutes, respectively. The transient response was plotted as the normalized change in electrical resistance $[\Delta R/R_0 \times 100 = (R_f - R_0)/R_0 \times 100]$ % of sensors as shown in Figure 1a, where R_f is the peak resistance and R_0 is the initial baseline resistance prior to analyte exposure. The $\Delta R/R_0$ increased to a steady-state during H_2 exposure and returned to its initial baseline when switching H_2 back to dried air. Figure 1b presents the plot of $\Delta R/R_0$ as a function of H_2 concentration showing a logarithmic function relationship. The inset in Figure 1b depicts the plot of $\Delta R/R_0$ as a function of H_2 concentration on a semi-log scale, yielding a rather straight line given by $\Delta R/R_0$ (%) = 3.440 × Ln ([H_2]) − 8.584 with a correlation coefficient R^2 = 0.9987. This relationship projects $\Delta R/R_0$ (%) ≈ 2.5% at 25 ppm_v exposure.

Additionally, the response and recovery times are important key factors when evaluating the overall sensing performance. In general, the response time τ_{90} and the recovery time τ_{90} are calculated, which are defined as the time for the sensor to reach 90% of its steady-state value and the time required for the sensor to return to 10% of its maximum response. However, the recovery time τ_{50}, which indicates the time needed for the sensor response to restore 50% of its maximum response, is chosen for sensor performance evaluation owing to slow recovery rates against rapid cycling of H_2 concentration. Figure 1c,d illustrated the sensor response time τ_{90} and recovery time τ_{50} at room temperature as a function of H_2 concentration. The average response time for the Pd–SWNTs sensor was determined to be 10 min at H_2 concentration of 50 ppm_v. The response time decreased rapidly to 1.13 min at H_2 concentration of 2000 ppm_v. A trend line of average response time τ_{90} as a logarithmic function of H_2 concentration for the Pd-sensor gives τ_{90} = −2.43 × Ln ([H_2]) + 19.47 with a R^2 = 0.9989. Extrapolating to 25 ppm_v of H_2 gas gives an average response time τ_{90} = 11.8 minutes. The average recovery time τ_{50} was also reduced from 12.28 min at 50 ppm_v to 0.37 min at 2000 ppm_v of H_2. Complete recovery was observed after the final H_2 exposure with recovery time τ_{100} of 30 min at 2000 ppm_v.

The sensing performance $(\Delta R/R_0 \times 100)$% of Pd–SWNTs aligned sensor to H_2 gas exposure is contrasted with other aligned SWNTs made with Pt, Cr, and Au microelectrodes in Figure 2a–c, respectively. The response of the Pt–SWNTs aligned sensor shown in Figure 2a is mainly attributed to the catalytic properties of Pt toward H_2 adsorption. The adsorbed hydrogen atoms exothermically react with oxygen molecules or weakly adsorbed oxygen atoms on the Pt surface, leading to hydroxyl radicals and/or water formation. The local heating from this catalytic reaction is considered to be a major contributor to the sensing response. However, this exothermic reaction was not activated until H_2 concentration exceeded 250 ppm_v, and a very pronounced response (i.e., $\Delta R/R_0$ = 8.98%) was obtained at 2000 ppm_v of H_2 gas. The drawback to the Pt–SWNT aligned sensor is its slow response and recovery time due to the slow gas adsorption processes at room temperature. Even though the Cr–SWNT aligned sensor gave about the same response ($\Delta R/R_0 \approx 2.5\%$) at 250 ppm_v of H_2 gas as the Pt–SWNT aligned sensor, the Cr-sensor's signal was more

dx.doi.org/10.1021/am404328g | ACS Appl. Mater. Interfaces 2014, 6, 319–326

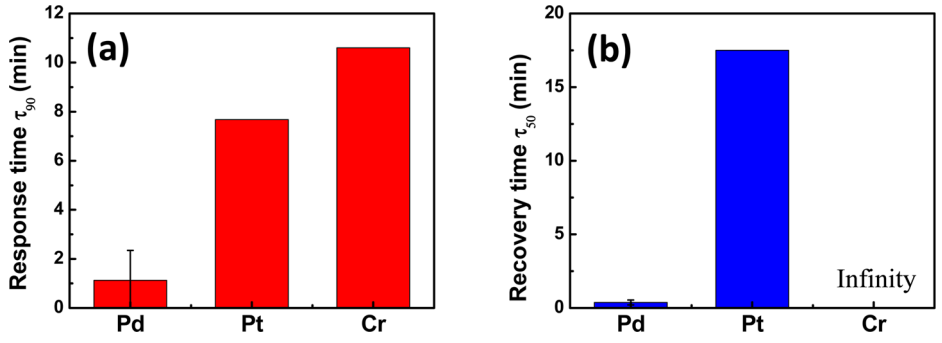

Figure 3. (a) Response time and (b) recovery time of AC aligned SWNTs on Pd, Pt, and Cr electrodes towards 2000 ppm_v H_2. No recovery time for Cr electrodes is included.

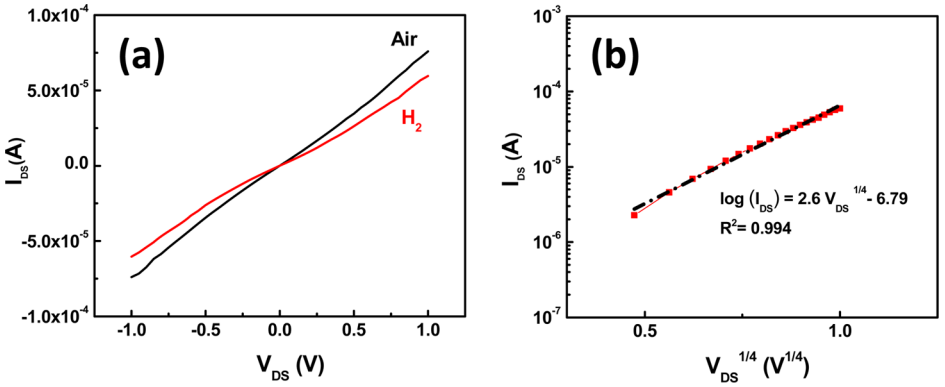

Figure 4. (a) Current (I_{DS}) − voltage (V_{DS}) and (b) I_{DS} − $V_{DS}^{1/4}$ characterization of AC aligned SWNTs on Pd electrodes in air (black) and 2000 ppm_v H_2 (red).

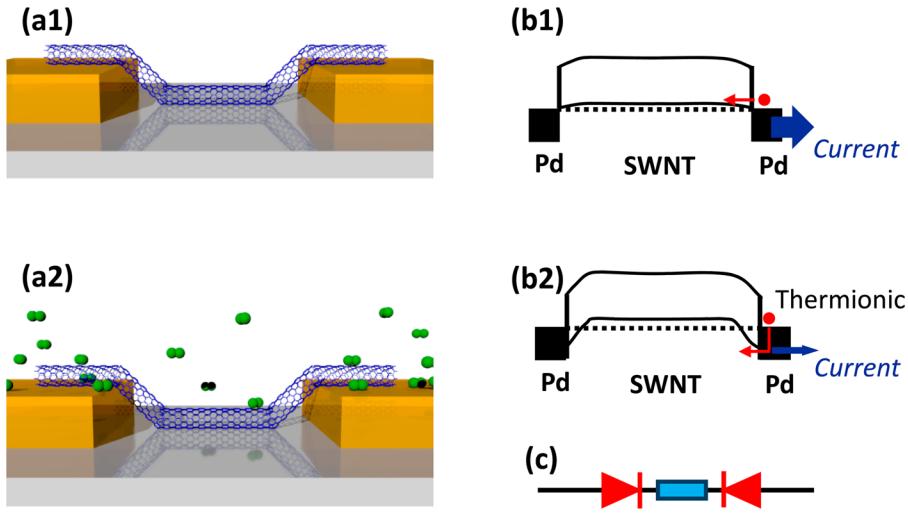

Figure 5. (a) Schematic representation (b) band diagram, and (c) equivalent circuit of SWNT devices in air (1) and H_2 (2).

distinct (less noisy). The Cr sensor also gave a larger response than the Pt sensor at 2000 ppm_v of H_2 gas, with $\Delta R/R_0$ = 14.54% vs 9%, respectively. The sensor response of this device is expected to be controlled by the trade-off between the resistance decrease induced by the reduction of the native oxide layer and the resistance increase from the CrH_x formation. Once the sensor is exposed under H_2 gas, reduction of the native oxide layer on the surface of the Cr electrode will release the oxygen bonded electrons, increasing the electron concentration and decreasing the resistance. On the other hand, H_2 is anticipated to cause an increase in the Fermi energy of Cr, therefore, decreasing its work function.[19] This leads to an augment in the SBH at the Cr−SWNT interface, resulting in the resistance to increase. In our work, Schottky becoming "Schottkier" is considered to be the key factor to generate a distinct positive sensor response, because the native oxide layer on the surface of the Cr electrode is normally too thin to produce any well-defined negative response. Note, however, that the Cr-sensor exhibited no recovery after exposed to 250 ppm_v of H_2 gas and showed two distinguishable recovery rates in the higher H_2 concentration region. The plateaued $\Delta R/R_0$ region indicates that an irreversible process happened on the

dx.doi.org/10.1021/am404328g | ACS Appl. Mater. Interfaces 2014, 6, 319−326

surface of the Cr electrode, such as a hydrogenation. Due to the much lower solubility of hydrogen in Cr than Pd, poorer performance was observed in the Cr−SWNT aligned device than Pd−SWNT. The Au−SWNT aligned sensor showed an insignificant response at all tested H_2 concentrations.

Figure 2d shows the $(\Delta R/R_0 \times 100)\%$ response calibration curve of the four (i.e., Pd, Pt, Cr, Au) SWNT aligned chemiresistive H_2 sensors, and the corresponding response/recovery times plotted, as histograms referenced at 2000 ppm_v of H_2 gas, are shown in Figure 3. The response time of the Pd sensor was 8 times faster than the Pt sensor and about 11 times faster than the Cr sensor, whereas the recovery time of the Pd sensor was 46 times faster than the Pt sensor and the Cr sensor never did recover. This substantiated that aligned SWNTs bridged Pd microelectrodes had high affinity toward H_2 gas and outperformed other fabricated sensors in this study.

To confirm that the superior sensing performance from the Pd−SWNT was primarily from the SB modulation at the metal−semiconductor interface, electrical characterizations of the sensors were performed. Room temperature $I-V_{sd}$ characteristics show a linear response for SWNTs in air and a nonlinear, S-shaped $I-V$ curve when the sensor was exposed to 2000 ppm_v of H_2 gas (Figure 4a). An ohmic contact was anticipated at the Pd interface and SWNT due to the larger work function of Pd (5.22 eV[20]) than that of SWNT (5.05 eV[21]). This assumption was corroborated by the experimentally obtained linear $I-V$ characteristic in air. During H_2 adsorption, atomic hydrogen is believed to dissolve into the Pd. Formation of Pd−H rapidly lowers the electronic work function (i.e., ~0.4 eV) and creates a SB at the interfacial Pd−SWNT contact.[22] Figure 5 shows the schematic diagrams of the sensor device and the band diagrams of Pd−SWNT−Pd contacts, demonstrating an equivalent back-to-back Schottky circuit.

Among those back-to-back Schottky configurations where the thermionic emission rule applies, three models were frequently observed with regard to the number of MS interfaces considered as well as the direction of the current flow. Some papers (Model 1) treated back-to-back Schottky as a Schottky diode where only one forward current is counted to calculate the total current whereas other papers (Model 2) considered the total current is a sum of two forward biased currents. In this paper[12] (Model 3), the total current is considered to be limited only by the reverse biased junction because this is the true bottleneck of the current. The reverse current can be explained by the following equations:

$$I_r = I_s = AA^*T^2\exp\left(\frac{-q\varphi_b}{kT}\right) \quad (1)$$

with

$$\varphi_b = \varphi_0 - \sqrt{\frac{qE}{4\pi\varepsilon\varepsilon_0}} \quad (2)$$

and

$$E = \sqrt{\frac{2qN_D}{\varepsilon\varepsilon_0}\left(V_0 + V_{bi} - \frac{kT}{q}\right)} \quad (3)$$

where I_r is the total current equal to the saturation current, $A^* = 4\pi m^* k^2/h^3$ is the effective Richardson constant, A is the cross section of the effective area perpendicular to the current, φ_b is the effective barrier height, φ_0 is the ideal barrier height, V_0 is the bias voltage, and $V_{bi} = \phi_b - \xi$ is the built-in potential, with ξ being the energy of the Fermi level of the semiconductor measured from the bottom of the conduction band.

From these equations, the logarithm of the reverse thermionic current must be linear to the 4th root of bias voltage, as shown in the Figure 4b. Hence, the reverse thermionic emission current gives a satisfactory explanation of the experimental results. However, the SBH is not able to be extracted from a single $I-V$ measurement because neither the effective Richardson's constant nor the electrically active area of SWNT is known.[17]

FET characterization was carried out to confirm the SB based sensing mechanism in the Pd−SWNT system. Typical FET $I_{ds} - V_g$ curves in dry air and H_2 gas are shown in Figure 6.

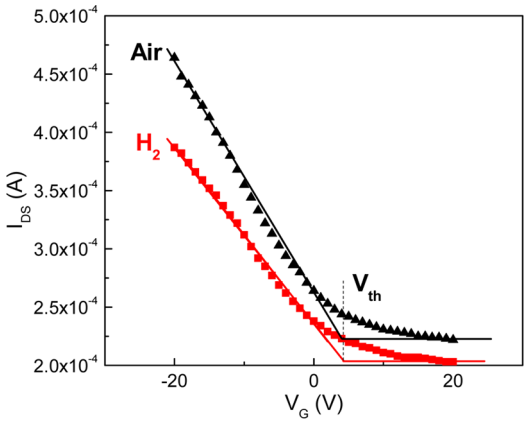

Figure 6. Current (I_{SD}) − back gated voltage (V_G) characterization of AC aligned SWNT on Pd electrodes in air (black triangle) and 2000 ppm H_2 (red square).

Notably, a decrease in source-drain current after exposure to H_2 gas was observed irrespective of the gate voltages. This is consistent with the anticipated decrease in p-channel conductance due to the SB formation at Pd−SWNTs interface upon exposure to H_2. If the charge transfer and chemical doping of the transducer is modulated by the gas molecules, an ion gating effect is anticipated as a sensing mechanism, resulting in a change in device carrier concentration with no change in its mobility.[23] In contrast, if an electrostatic gating effect becomes the dominating sensing mechanism, the charge transfer between a sensitive element and gas analyte or chemical doping caused by gas molecules would alter the sensor's carrier concentration. Therefore, a redistribution of the charge carriers therefore reflects a shift in $V_{th,}$ while transconductance (i.e., carrier mobility) remains unchanged.

The carrier mobility was calculated using the following equations:[24]

$$\mu = \frac{L_{SD}W_{SD}\left(\frac{dI}{dV_G}\right)}{C_G V_{SD}} \quad \text{(Eq. 4)}$$

with

$$C_G = \frac{\varepsilon\delta(L_{SD})(W_{SD})}{t_{DL}} \quad \text{(Eq. 5)}$$

where μ is the carrier mobility ($cm^2/(Vs)$), L_{SD} is the length of the SWNT or the electrodes' gap size (3 μm), W_{SD} is the width of the CNT film (10 μm), dI/dV_G is the transconductance (A/V), C_G is the capacitance (F), V_{SD} is the applied source-drain

dx.doi.org/10.1021/am404328g | ACS Appl. Mater. Interfaces 2014, 6, 319−326

Table 1. Characteristics of Various Pd−CNT (Graphene)-Based Room Temperature H_2 Sensors

	sensor configuration				sensing performance						
category	substrate	electrode	transducer	Pd decoration	dynamic range (ppm)	sensitivity (% ppm^{-1})	τ_{90} (min)	τ_{50} (min)	@ H_2 concentraion (%)	LDL# (ppm)	year
1	S[a]	Pd	aligned SWNTs	N/A	$25-2\times10^3$	0.074	1.1	0.37	0.2	25	this work
	S	Pd	single SWNT	N/A	$5\times10^3-5\times10^5$	0.020					2003[10]
	Si	Pd	CNT film	N/A		1.1×10^{-4}					2003[26]
	S	Au	graphene	N/A	$50-1\times10^4$	6.8×10^{-3}	0.94	0.40	0.2	50	2013[27]
2	S	Au/Ti	single SWNT	NPs		0.12	0.1	3.3	0.04	<40	2001[42]
			SWNT film			0.060	0.3	3.3	0.04	<40	
	S	Pd	SWNT film	NPs	10−500	0.29	14		0.05	10	2005[28]
	Al_2O_3	Au	SWNT film	NPs	$5\times10^3-4\times10^4$	2.0×10^{-3}	6.0	12.1	0.5	<5000	2005[15]
	glass	Cr	SWNTs	NPs	$100-1\times10^4$	1.0×10^{-4}	5.3	2.9	0.1	<100	2007[43]
	PET	Pd/Ti	SWNTs	CLs[b]	$30-1\times10^4$	0.10	0.48	0.17	0.1	30	2007[44]
	S	Au/Ti	SWNT film	NPs	$100-3\times10^3$	0.42	11.2	57	0.2	100	2007[22]
	PET	Pd/Ti	SWNTs	CLs	$100-1\times10^4$	0.26	1.11		0.1	100	2008[45]
	S	Pd/Ti	single SWNT	NPs		0.06	0.095	0.62	100		2010[30]
	Al_2O_3	Pt	SWNT film/ SiO_2	NPs	1−100	0.21	0.17		0.01	1	2011[46]
		Fl[c]	MWNT yarns	CLs	$20-4\times10^4$	6.0×10^{-3}	2.3	0.68	0.1	20	2012[47]
	S	Au	DWNTs	NPs	$500-3\times10^4$	0.018	0.75	0.45	0.1	<500	2012[48]
			CNT paper	NPs		-7.7×10^{-5}	1.9	0.54	5	360	2012[49]
	glass	Pt	CNT/Ni film	NPs	$200-1.6\times10^4$	1.4×10^{-3}	1.9×10^{-3}	0.038	0.2	200	2012[50]
	S	Au/Ti	SWNTs/ DNA	NPs	$100-2\times10^3$	0.5	10.6	1.6	0.1	100	2013[33]
	S	Au	MWNT array	NPs	$500-1\times10^4$	2.8×10^{-4}	1.9	0.54	0.1	<500	2013[51]
	S	Au	graphene	NPs	$1-1\times10^3$	0.027	0.90	4.62	0.1	1	2013[52]
	S	Au	SWNT film	NPs	$250-2.5\times10^4$	5.8×10^{-4}	2.5		0.25	250	2013[53]

[a]S: Si/SiO_2 substrate. # LDL: lowest detection limit. [b]CLs: clusters. [c]Fl: filament, @ H_2 conc. (%) means at which H_2 concentration the response/recovery time was determined.

voltage (V), ε is the permittivity constant ($8.85\times10^{-12}\ F/m$), δ is the dielectric constant of SiO_2 ($\delta = 3.9$[25]), and t_{DL} is the thickness of the dielectric layer (300 nm). A mobility change of 23.2% was calculated. This result is consistent with the sensing data.

Table 1 compares this work with the literature reported Pd−CNT (graphene)-based room temperature H_2 sensors, including the sensors' configurations and sensing performance (i.e., dynamic range, sensitivity, response/recovery time, and lowest detection limit (LDL)). These sensors were grouped into two categories, depending on whether the transducer (i.e., CNT, graphene) was decorated with Pd (Category 2) or without (Category 1). Category 1 includes sensors that are based on either a single Schottky diode[26,27] or a back-to-back Schottky contact.[10] Their gas sensing response is mainly attributed to the modulation of metal−semiconductor (MS) contacts in the interface of electrode and transducer. For Category 2, Pd nanoparticles (NPs) or clusters are functionalized to a single CNT, CNT array, or CNT films. Modulation in the conductance of the transducer rather than the MS contact was dominated during the gas detection, due to the local SBH change induced by the Pd on the transducer upon the H_2 gas exposure.

Sensors obtained in this work show the best sensitivity among the Pd−CNT based H_2 gas sensors in Category 1; our sensitivity is slightly higher than that of the Pd-single SWNT-based device [10] but 1 or 2 orders higher than that from SWNT films[28] and graphene.[27] In a single SWNT, a sensitivity of 0.02 % ppm^{-1} was achieved upon exposure to 0.5% of H_2 gas, with the presence of −5 V gate voltages. Sensitivity without the gate voltage cannot be quantified here due to the resolution of the figures provided but should definitely be higher than 0.02 % ppm^{-1} owing to the diminished tunneling effect. SWNTs used in this study are carboxylated SWNTs, which contain carboxylated defects and stone-wall defects.[29] Higher sensitivity obtained in our work may be due to the presence of defects in the SWNTs at the Pd/SWNT contact region, forming a defect-Pd−H_2 system, which therefore, augment the sensing performance.[30] More detailed explanation will be given in a following paragraph of this paper.

In a SWNT film or network, the presence of a mixture of metallic (m-SWNTs) and semiconducting SWNT (s-SWNT) is expected. Hence, the carriers are more likely to flow though the m-SWNT, where no SB is constructed,[31] and bypass the barrier within the metal-s-SWNT contact, in accordance with the parallel resistor law. This leads to attenuation in the signal and lower the sensitivity of the sensor. In addition, the interactions of adjacent aligned CNTs may lead to carrier screening effects, hopping, or even Schottky junctions as semiconducting and metallic tubes cross each other,[32] therefore altering the carrier transport behavior and the sensing performances. A stronger "bypass" effect and interaction are anticipated in a CNT film, rather than the aligned SWNTs in this work (a mixture of m-SWNTs and s-SWNTs with a ratio of 1:2), which leads to a diminished sensitivity in the film sample.

Compared to the sensors in Category 1, the Pd decorated SWNTs (Category 2) show an improved sensing performance. The highest sensitivity, almost 1 order higher than that of this work, was obtained in a Pd and DNA cofunctionalized SWNT based device.[33] The Pd NPs are not only considered as the

catalyst to oxidize the H_2 to H_2O but also function as nanogate electrodes to scatter the carriers in the SWNTs. Therefore, the electrical resistance of the sensor can be altered significantly and its magnitude increases with the number of Pd NPs.[33] SWNT films that are electrochemically functionalized by Pd NPs also have a high sensitivity toward H_2 gas.[22] This could be attributed to the alteration of the electronic work function of the Pd upon the gas exposure, which leads to the modulation of the local SBs in the interface of Pd NPs and SWNTs, thereby resulting in the sensors' electrical resistance change.

Presence of defects at the Pd/SWNT interfaces can also enhance the sensitivity. It is known that defects can alter the electronic properties of SWNTs because they can significantly limit the mean free path of the carriers, thereafter creating a potential drop along the SWNTs.[34] When exposed to gases, even though the adsorption of gas molecules (i.e., NH_3) on defective SWNTs are known to be easier than on defect-free SWNTs,[35] both of the defective and defect-free SWNTs are reported to show no difference when exposed to H_2 gas.[30] However, Pd coverage on the defect has extraordinary consequences on the improvement of the sensitivity towards H_2 gas, showing a 1000-fold increase in resistance change. The author attributed this augmentation to a specific interdependence between defect sites' electronic transmission and the chemistry of the defect-Pd−H_2 system.[30] The effect of defects was also observed in the electrochemically functionalized SWNT films, where a superior sensitivity, over those are synthesized by vacuum evaporation and sputtering, was observed.[22]

In addition, existence of SBs within a CNT, except for between the metal contact and the CNT, may increase the sensitivity. When contacted with Pd, the local density of state of the SWNTs exhibits substantial hybridization between the SWNT and metal surfaces.[36] In this case, no potential barrier exists between the SWNTs and the Pd surface. This implies that the SWNTs are no longer acting as semiconductors once they are contacted with Pd. Therefore, any SB present would be between a metallic-like and a semiconducting segment in the same CNT.[37,38] Those barriers are hosted along the CNT and can be altered upon the gas exposure, thereby modulating the electrical resistance of the sensor assembly.

Even though the sensitivity of SWNTs increases significantly by the Pd decoration, their sensing performances are still poorer than those are based on other semiconductors, such as these Si,[13] ZnO,[39] and AlGaN.[40] Those sensors are based on either a single Schottky diode[39,40] or a back-to-back Schottky contact.[13] It is expected that superior sensing performances will be obtained from a CNT-based sensor, because the SBH should be fully controlled by the metal work function in a metal−CNT contact as opposed to most bulk metal−semiconductor junctions. However, in a side-contacted CNT where the depletion region extends perpendicular to the main axis of CNT, there is only a short available distance in which the band can realign to equilibrate the Fermi levels.[32] Therefore, only partial band realignment is possible, which will introduce pinning to the surface of the CNT, causing the work function control over SBH to fail. In addition, an even stronger pinning effect is expected when a CNT is chemically functionalized with foreign groups. Because the chemical groups (i.e., carboxylic groups in this work) are mainly localized at the edges of the CNT, the interface states in the metal−CNT contact area are anticipated to increase. This will drive the junction's performance away from the Schottky−Mott limit and result in Fermi level pinning. Therefore, pinning should still be taken into consideration in this work and be regarded as one of the main factors that weaken the control over SBH from the metal's work function, consequently resulting in reduced sensing response.

Furthermore, electron tunneling may be another factor that alters the sensing performance of CNTs. In 2-D films or 1-D structures with large diameters, doping or a high gate voltage is necessary to narrow the SB width and then activate the carrier tunneling. However, doping or a high gate voltage are not essential in CNTs due to its exceptionally small diameter (~1.4 nm) because the SB width can be narrowed by the internal electric field, which is focused across the barrier. In other words, the effective SBH that an electron can "see" is lowered in the CNT because the electrons can tunnel though the SB instead of "jump" over the barrier. In our work, the tunneling effect is expected from the $I-V^{0.25}$ plot shown in Figure 4b, where the correlation coefficient (<1) shows a deviation of the device's behavior from the pure thermionic transport. In addition, extra carriers, which are induced by either the intrinsic defects in our CNTs or the chemical functionalization processes, will further increase the possibility of tunneling effect.[12]

Finally, the crystallographic structure of the metal surface is essential in determining a SBH.[41] Because the Pd electrodes in this work are synthesized by e-beam evaporation, they are polycrystalline with an average grain size of about 15−20 nm. In this case, a nonuniform Fermi level is likely to position at the Pd/SWNT interface, leading to the construction of nonuniform SBHs. Variations in the modulation of these nonuniform SBHs, which deviate the sensing performances from sample to sample, explain the non-negligible error bars in the Figure 1b.

4. CONCLUSIONS

Chemiresistive H_2 gas sensors were fabricated using SWNTs as transducers bridged across various metal (e.g., Pd, Pt, Au, and Cr) microelectrodes. The chemiresistive sensors with Pd−SWNTs combination in this study demonstrated a significantly higher sensitivity with notably faster response and recovery times as compared to other Pd−CNT sensors fabricated. $I-V$ characteristic of the sensors was fitted with a back-to-back SB configuration, where the reverse thermionic emission current gives a satisfactory explanation of the experimental results. The formation of Pd−H at the Pd−SWNT contacts lowers the work function of Pd, thus modulating the SBH after electronic band rearrangement. The sensors configured as FETs corroborates that modulation of the SBH at the interfacial Pd−SWNT dominates the sensing mechanism toward H_2 adsorption with a distinct signature (i.e., a decrease in carrier mobility without a change in carrier concentration).

AUTHOR INFORMATION

Corresponding Author

*N. V. Myung. E-mail: myung@engr.ucr.edu. Address: Department of Chemical and Environmental Engineering at University of California—Riverside, Bourns Hall B353, 900 University Avenue, Riverside, CA 92521.

Notes

The authors declare no competing financial interest.

■ ACKNOWLEDGMENTS

This research work was supported by the Fundamental R&D Program for Core Technology of Materials funded by the Ministry of Knowledge Economy, Republic of Korea.

■ REFERENCES

(1) Gu, H. S.; Wang, Z.; Hu, Y. M. *Sensors (Basel)* **2012**, *12*, 5517−5550.
(2) Hubert, T.; Boon-Brett, L.; Black, G.; Banach, U. *Sens. Actuators, B* **2011**, *157*, 329−352.
(3) Qurashi, A.; Yamazaki, T.; El-Maghraby, E. M.; Kikuta, T. *Appl. Phys. Lett.* **2009**, *95*, 153109.
(4) Wang, B.; Zhu, L. F.; Yang, Y. H.; Xu, N. S.; Yang, G. W. *J. Phys. Chem. C* **2008**, *112*, 6643−6647.
(5) Huh, J.; Park, J.; Kim, G. T.; Park, J. Y. *Nanotechnology* **2011**, *22*, 085502.
(6) Steinebach, H.; Kannan, S.; Rieth, L.; Solzbacher, F. *Sens. Actuators, B* **2010**, *151*, 162−168.
(7) Jun, Y. K.; Kim, H. S.; Lee, J. H.; Hong, S. H. *Sens. Actuators, B* **2005**, *107*, 264−270.
(8) Favier, F.; Walter, E. C.; Zach, M. P.; Benter, T.; Penner, R. M. *Science* **2001**, *293*, 2227−2231.
(9) Flanagan, T. B.; Oates, W. A. *Annu. Rev. Mater. Sci.* **1991**, *21*, 269−304.
(10) Javey, A.; Guo, J.; Wang, Q.; Lundstrom, M.; Dai, H. J. *Nature* **2003**, *424*, 654−657.
(11) Zhao, Z.; Carpenter, M. A.; Xia, H.; Welch, D. *Sens. Actuators, B* **2006**, *113*, 532−538.
(12) Spyropoulos-Antonakakis, N.; Sarantopoulou, E.; Kollia, Z.; Samardzija, Z.; Kobe, S.; Cefalas, A. C. *J. Appl. Phys.* **2012**, *112*, 094301.
(13) Skucha, K.; Fan, Z. Y.; Jeon, K.; Javey, A.; Boser, B. *Sens. Actuators, B* **2010**, *145*, 232−238.
(14) Yamamoto, N.; Tonomura, S.; Matsuoka, T.; Tsubomura, H. *Surf. Sci.* **1980**, *92*, 400−406.
(15) Schierbaum, K. D.; Kirner, U. K.; Geiger, J. F.; Gopel, W. *Sens. Actuators, B* **1991**, *4*, 87−94.
(16) Hersam, M. C. *Nat. Nanotechnol.* **2008**, *3*, 387394.
(17) Svensson, J.; Campbell, E. E. B. *J. Appl. Phys.* **2011**, *110*, 111101.
(18) Zhang, M. L.; Su, H. C.; Rheem, Y.; Hangarter, C. M.; Myung, N. V. *J. Phys. Chem. C* **2012**, *116*, 20067−20074.
(19) Szadkowski, A. J.; Kalnitsky, A.; Ma, K. B.; Zukotynski, S. *J. Appl. Phys.* **1982**, *53*, 557−558.
(20) *CRC Handbook of Chemistry and Physics*; Lide, D. R., Ed.; CRC Press: Boca Raton, FL, 2003.
(21) Shiraishi, M.; Ata, M. *Carbon* **2001**, *39*, 1913−1917.
(22) Mubeen, S.; Zhang, T.; Yoo, B.; Deshusses, M. A.; Myung, N. V. *J. Phys. Chem. C* **2007**, *111*, 6321−6327.
(23) Mubeen, S.; Lim, J. H.; Srirangarajan, A.; Mulchandani, A.; Deshusses, M. A.; Myung, N. V. *Electroanalysis* **2011**, *23*, 2687−2692.
(24) Martel, R.; Schmidt, T.; Shea, H. R.; Hertel, T.; Ph, A. *Appl. Phys. Lett.* **1998**, *73*, 2447−2449.
(25) Gray, P. R.; Hurst, P. J.; Lewis, S. H.; Meyer, R. G. *Analysis and Design of Analog Integrated Circuits*; Wiley: New York, 2009; Vol. *40*.
(26) Wong, Y. M.; Kang, W. P.; Davidson, J. L.; Wisitsora-at, A.; Soh, K. L. *Sens. Actuators, B* **2003**, *93*, 327−332.
(27) Lim, J.; Hwang, S.; Yoon, H. S.; Lee, E.; Lee, W.; Jun, S. C. *Carbon* **2013**, *63*, 3−8.
(28) Sippel-Oakley, J.; Wang, H. T.; Kang, B. S.; Wu, Z. C.; Ren, F.; Rinzler, A. G.; Pearton, S. J. *Nanotechnology* **2005**, *16*, 2218−2221.
(29) Fan, Y. W.; Goldsmith, B. R.; Collins, P. G. *Nat. Mater.* **2005**, *4*, 906−911.
(30) Khalap, V. R.; Sheps, T.; Kane, A. A.; Collins, P. G. *Nano Lett.* **2010**, *10*, 896−901.
(31) Kim, W.; Javey, A.; Tu, R.; Cao, J.; Wang, Q.; Dai, H. *J. Appl. Phys. Lett.* **2005**, *87*, 173101.
(32) Mustonen, T.; Maklin, J.; Kordas, K.; Halonen, N.; Toth, G.; Saukko, S.; Vahakangas, J.; Jantunen, H.; Kar, S.; Ajayan, P. M.; Vajtai, R.; Helisto, P.; Seppa, H.; Moilanen, H. *Phys. Rev. B* **2008**, *77*, 125430.
(33) Su, H. C.; Z., M.; Bosze, W.; Lim, J. H.; Myung, N. V. *Nanotechnology* **2013**, *24*, 505502.
(34) Freitag, M.; Tsang, J. C.; Bol, A.; Yuan, D. N.; Liu, J.; Avouris, P. *Nano Lett.* **2007**, *7*, 2037−2042.
(35) Peng, N.; Zhang, Q.; Chow, C. L.; Tan, O. K.; Marzari, N. *Nano Lett.* **2009**, *9*, 1626−1630.
(36) Takagi, Y.; Okada, S. *Phys. Rev. B* **2011**, *84*, 035406.
(37) Okada, S.; Oshiyama, A. *Phys. Rev. Lett.* **2005**, *95*, 206804.
(38) Zhu, W. G.; Kaxiras, E. *Nano Lett.* **2006**, *6*, 1415−1419.
(39) Basu, S.; Dutta, A. *Mater. Chem. Phys.* **1997**, *47*, 93−96.
(40) Chang, C. F.; Tsai, T. H.; Chen, H. I.; Lin, K. W.; Chen, T. P.; Chen, L. Y.; Liu, Y. C.; Liu, W. C. *Electrochem. Commun.* **2009**, *11*, 65−67.
(41) Shan, B.; Cho, K. J. *Phys. Rev. B* **2004**, *70*, 233405.
(42) Kong, J.; Chapline, M. G.; Dai, H. J. *Adv. Mater.* **2001**, *13*, 1384−1386.
(43) Suehiro, J.; Yamane, S.; Imasaka, K. In *Sensors*; IEEE, 2007; pp 554−557.
(44) Sun, Y. G.; Wang, H. H. *Adv. Mater.* **2007**, *19*, 2818−2823.
(45) Sun, Y. G.; Wang, H. H.; Xia, M. G. *J. Phys. Chem. C* **2008**, *112*, 1250−1259.
(46) Wongwiriyapan, W.; Okabayashi, Y.; Minami, S.; Itabashi, K.; Ueda, T.; Shimazaki, R.; Ito, T.; Oura, K.; Honda, S.; Tabata, H.; Katayama, M. *Nanotechnology* **2011**, *22*, 055501.
(47) Randeniya, L. K.; Martin, P. J.; Bendavid, A. *Carbon* **2012**, *50*, 1786−1792.
(48) Rumiche, F.; Wang, H. H.; Indacochea, J. E. *Sens. Actuators, B* **2012**, *163*, 97−106.
(49) Ventura, D. N.; Li, S.; Baker, C. A.; Breshike, C. J.; Spann, A. L.; Strouse, G. F.; Kroto, H. W.; Acquah, S. F. A. *Carbon* **2012**, *50*, 2672−2674.
(50) Lin, T. C.; Huang, B. R. *Sens. Actuators, B* **2012**, *162*, 108−113.
(51) Yick, S.; Yajadda, M. M. A.; Bendavid, A.; Han, Z. J.; Ostrikov, K. *Appl. Phys. Lett.* **2013**, *102*, 233111.
(52) Phan, D.-T.; Chung, G.-S. *Int. J. Hydrogen Energy* **2014**, *39*, 620−629.
(53) Lee, J.-H.; Kang, W.-S.; Najeeb, C. K.; Choi, B.-S.; Choi, S.-W.; Lee, H. J.; Lee, S. S.; Kim, J.-H. *Sens. Actuators, B* **2013**, *188*, 169−175.